Lunar Global Shape and Polar Topography Derived from Kaguya-LALT Laser Altimetry

H. Araki,[1]* S. Tazawa,[2] H. Noda,[1] Y. Ishihara,[2] S. Goossens,[2] S. Sasaki,[2] N. Kawano,[2] I. Kamiya,[3] H. Otake,[4] J. Oberst,[5] C. Shum[6]

A global lunar topographic map with a spatial resolution of finer than 0.5 degree has been derived using data from the laser altimeter (LALT) on board the Japanese lunar explorer Selenological and Engineering Explorer (SELENE or Kaguya). In comparison with the previous Unified Lunar Control Network (ULCN 2005) model, the new map reveals unbiased lunar topography for scales finer than a few hundred kilometers. Spherical harmonic analysis of global topographic data for the Moon, Earth, Mars, and Venus suggests that isostatic compensation is the prevailing lithospheric support mechanism at large scales. However, simple rigid support is suggested to dominate for the Moon, Venus, and Mars for smaller scales, which may indicate a drier lithosphere than on Earth, especially for the Moon and Venus.

Knowledge of the lunar shape and topography is fundamental for our understanding of the internal structure and surface evolution of the Moon. However, laser topographic mapping of the Moon had been limited. Early experiments were carried out by the Apollo 15 to 17 spacecraft for limited areas below their near-equatorial orbits (*1*). More recently, laser altimeter on the Clementine obtained topographic data covering almost the entire South Pole–Aitken Basin (*2*). Its coverage did not reach beyond 80° latitude owing to the elliptic orbit of the spacecraft, and the spatial resolution is 20 to 60 km (*3*). A full topographic map, including the polar regions, ULCN 2005, was produced using photogrammetric analysis of Clementine images combined with data from historical control points on the Moon (*4*). However, the map is known to suffer from large systematic errors. Radar topography from Earth includes gaps due to limitations of viewing and illumination conditions, whose effects are especially evident in the polar regions (*5*, *6*).

The LALT on board the Japanese lunar explorer Kaguya (SELENE) is designed to measure distances to the lunar surface from the altitude of 100 km (*7*). LALT measures the distance from the spacecraft to the surface of the Moon by transmitting Nd and Cr-doped yttrium-aluminum-garnet (Cr-doped Nd:YAG) laser pulses every second. The beam divergence is 0.4 milliradian, resulting in the laser spot size on the lunar surface of typically 40 m from the orbiter altitude of 100 km. To exploit the instrument's nominal range resolution of 1 m, the range data are calibrated for thermal variations of the internal clock frequency and the instrument delay. The errors related to data quantization, thermal variation of the clock and electronics, and instrument delay measurement are estimated to be 0.55 m (1 SD) (*8*, *9*). The first ranging tests were carried out successfully on 25 November 2007, and the nominal mapping phase began on 30 December 2007. Topography data were produced by incorporating precise orbits for the Kaguya main orbiter. These orbits are calculated from two-way Doppler data by the GEODYN-II software using the latest lunar gravity model SGM90em (SELENE Gravity Model) that is an adapted version of the model SGM90d for the purpose of orbit determination (*10*–*12*). Orbit precision is determined from orbit differences during overlapping parts, showing that the radial orbit error is generally within 1 m (*13*) and the total positioning error (computed using the root sum square over the radial, along-track, and cross-track directions) is found to be ~50 m. Thus, the radial topographic error originated from the orbit repeatability is 1 m (1 SD), the instrumental error is 0.55 m (1 SD), and the instrument range shift is between +2.5 m and +12 m (*8*, *9*), which are summarized ±4.1 m (1 SD) as the final budget where the range shift is incorporated as 4 m (1 SD). In the same way, the horizontal topographic error originated from the orbit repeatability is 50 m (1 SD), the pointing error is 175 m (maximum), and the time-tag error is 1.5 m (maximum), which are summarized as ±77 m (1 SD) as the final budget (*14*). Attitude and time-tag data are provided from the tracking and operation center of the Japan Aerospace Exploration Agency (JAXA). The number of geolocated points over the entire lunar surface is about 6.77×10^6 as of 31 March 2008 (*15*).

Figure 1 shows the topographic map obtained from LALT data. It clearly delineates the prom-

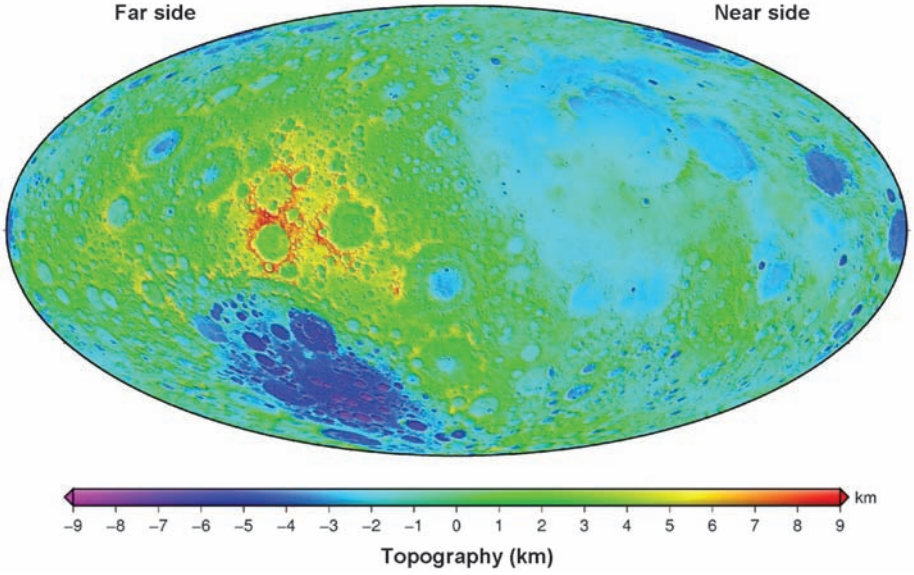

Fig. 1. Lunar global topographic map obtained from LALT altimetry data shown in Hammer equal-area projection. Lunar coordinates are based on the mean Earth/polar axis system. Reference of the height is a sphere whose radius is 1737.4 km and whose origin is set to the center of mass (*19*). The map center is 270°E, with the nearside on the right and the farside on the left. Full range of the topography is about 19.81 km. The highest point is on the southern rim of the Dirichlet-Jackson basin (–158.64°E, 5.44°N, +10.75 km), and the lowest point is inside Antoniadi crater (–172.58°E, 70.43°S, –9.06 km) in the South Pole–Aitken Basin.

[1]National Astronomical Observatory of Japan, 2-21-1 Osawa, Mitaka, Tokyo 181-8588, Japan. [2]National Astronomical Observatory of Japan, 2-12 Hoshigaoka, Mizusawa, Oshu, Iwate 023-0861, Japan. [3]Geographical Survey Institute, 1 Kitasato, Tsukuba, Ibaraki 305-0811, Japan. [4]Japan Aerospace Exploration Agency, 2-1-1 Sengen, Tsukuba, Ibaraki 305-8505, Japan. [5]German Aerospace Center (DLR), Rutherfordstraße 2, 12489 Berlin, Germany. [6]Ohio State University, School of Earth Sciences, 121 South Oval Mall, 275 Mendenhall Laboratory, Columbus, OH 43210, USA.

*To whom correspondence should be addressed. E-mail: arakih@miz.nao.ac.jp

inent lunar geologic landforms, especially the Feldspathic Highland Terrane (FHT), mare basins, and the South Pole–Aitken Basin Terrane (SPAT). Mare surfaces, which are covered with basaltic lava, are remarkably flat. Ridge systems have elevations of a few hundred meters. In Mare Serenitatis and Imbrium, for example, ridges form concentric circular patterns parallel to the outermost mare cliff. Complex sinusoidal ridges are also seen in Oceanus Procellarum and Mare Imbrium. These ridge systems may be formed by subsidence of the mare basalt modified by preexisting multiring or smaller topographic features (fig. S1).

Because Kaguya is in a polar orbit, surface trajectories appear approximately parallel at low latitudes, with cross-track spacing less than 0.5° (about 15 km at the equator) (fig. S2). In the polar regions, the nearest neighbor distance between ranged positions is no more than 2 km inside the region of 1° from the poles (fig. S2). A comparison between LALT and ULCN 2005 maps shows that the LALT topographic map far exceeds the ULCN 2005 in resolution and accuracy for features that are less than a few hundred kilometers across (fig. S3).

On the farside of the Moon, the mean difference of topography is 10 km between FHT and the SPAT (Fig. 1, and fig. S4). The highest point on the Moon is on the southern rim of the Dirichlet-Jackson basin, and the lowest one is in the Antoniadi crater in the SPAT. The full-range topography spans about 19.81 km, which is greater than the ULCN 2005 result of 17.53 km for the next highest and lowest points, the positions of which are generally identical to our highest and lowest points, with differences of less than a few degrees (Fig. 1) (*16*).

Observations by LALT provide the first polar maps with complete coverage (Fig. 2). Small depressions or craters are observed for the first time in the polar image. For example, our map of the South Pole region disclosed a crater, with a diameter of ~15 km, inside of de Gerlache crater and a topographic depression on the farside of Shackleton and de Gerlache craters. The new polar map will be a valuable asset for planning future lunar exploration, especially for the sun-lighting conditions.

We have developed a spherical harmonic model complete to degree and order 359 [STM359_grid-02 (SELENE Topography Model)] using the LALT topographic data as of 31 March 2008. Topographic data were interpolated and assembled to 0.0625° by 0.0625° gridded data, boxcar filtered and resampled to a 0.25° by 0.25° grid (*17*), and then converted to spherical harmonic coefficients (*18*). The N degree and order spherical harmonic model of the global topography H is given as follows:

$$H(\lambda,\varphi) = \sum_{l=0}^{N} \sum_{m=0}^{l} \overline{P}_{lm}(\sin\varphi)(\overline{C}_{lm} \cos m\lambda + \overline{S}_{lm} \sin m\lambda) \quad (1)$$

where φ and λ are the lunar-centric latitude and longitude, respectively, based on the mean Earth/polar axis system (*19*). $\overline{P}_{lm}$ is the normalized associated Legendre function of degree l and order m. $\overline{C}_{lm}$ and $\overline{S}_{lm}$ are normalized spherical harmonic coefficients with units in meters. Low degree and order coefficients (0, 1, and 2) are listed in Table 1. Considering our known ranging errors, C_{00}, the mean radius of the Moon is estimated to be 1737.15 ± 0.01 km. It is considered that the error of C_{00} resulting from the orbit and attitude errors is averaged to be small in total. The mean radius derived from ULCN 2005 is 1736.93 ± 2.1 km, which is in good agreement with our value (*16*). The COM-COF (center of mass–center of figure) offset is derived from the C_{1m} (m = 0, 1) as (–1.772, –0.731, 0.239) km along three axes in the mean Earth/polar axis coordinates or 1.93 km in total. The direction of the COM-COF vector is displaced 22.41°E from the prime meridian and 7.10°N from the equator on the farside. This is slightly north of the highest elevation point of the Moon, which suggests that irregular mass distribution associated with shifted COM-COF offset around the axis of lunar minimum moments of inertia is virtually compensated due to the variations in crustal thickness. Our results on the COM-COF offset generally agree with those obtained from Clementine LIDAR (light detection and ranging) altimetry (*3*). The polar and mean equatorial radii are derived to be 1735.66 km and 1738.64 km, respectively, from the lunar mean radius (1737.15 km) and C_{20} coefficient. The polar flattening is thus estimated to be 1/581.9 from the two radii.

We compared STM359_grid-02 with the ULCN 2005 spherical harmonic model developed using the same procedure as for STM359_grid-02. The amplitude spectrum, which is derived as the square root of the total sum of squares of the spherical harmonic coefficients for each degree (Fig. 3), are nearly identical for degree and order less than 30 (half wavelength scale is more than 180 km on the Moon). However, the STM359_grid-02 spectral amplitudes are larger by a factor of two or more for degree and order 100 or at smaller scales

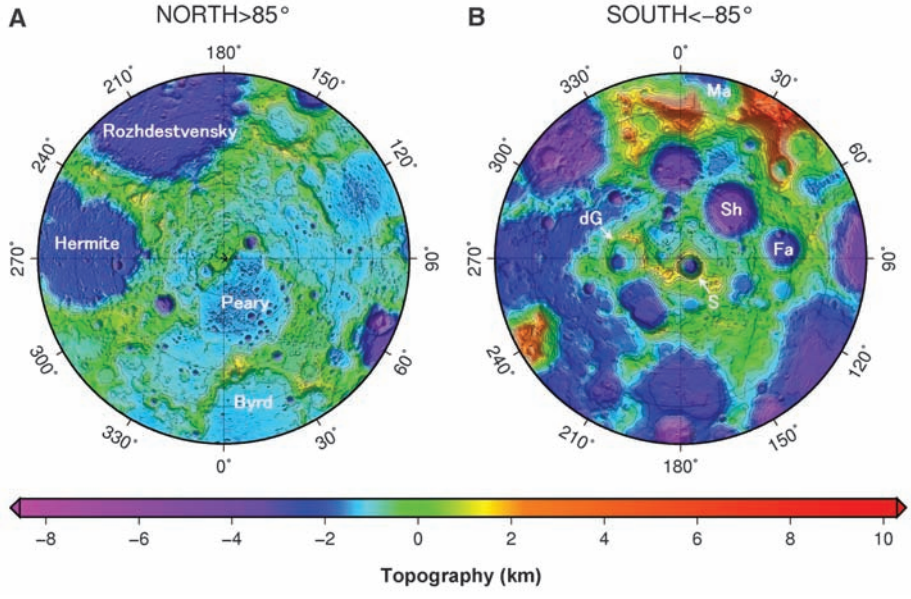

Fig. 2. Polar topographic maps of the Moon produced by LALT. The projections are stereographic for the North Pole (**A**) and the South Pole (**B**). Lunar coordinate system and the height reference are the same as Fig. 1. Some craters are labeled and some are abbreviated: Ma, Malapert; Sh, Shoemaker; Fa, Faustini; S, Shackleton; and dG, de Gerlache. The grid resolution is 0.015625° (1/64°) in latitude and 0.179° in longitude (0.473 km at 85°).

Table 1. Normalized coefficients of degree and order 0, 1, and 2, obtained from the lunar shape model (STM359_ grid-02) from the spherical harmonic analysis. Normalized associated Legendre function $\overline{P}_{lm}$ is $\overline{P}_{lm}(\sin\varphi) = \sqrt{(2l+1)(2-\delta_{l0})(l-m)!/(l+m)!}P_{lm}(\sin\varphi)$, where P_{lm} is an associated Legendre function. $\overline{P}_{lm}$ is used for our spherical harmonic analysis.

Degree: l	Order: m	$\overline{C}$ (m)	$\overline{S}$ (m)
0	0	1,737,156.3	—
1	0	137.9	—
1	1	–1023.2	–421.9
2	0	–668.1	—
2	1	–769.5	–16.9
2	2	109.2	383.4

(less than 55 km), indicating that the Moon is rougher at scales of less than 180 km than is indicated by ULCN 2005 model.

Topographic amplitude spectra T_p of the Moon and three terrestrial planets are compared in Fig. 4, where p is for the Moon (M), Mars (Ma), Venus (V), and Earth (E). T_M is calculated from STM359_grid-02, and T_{Ma}, T_V, and T_E are from results of spherical harmonic analysis of the three bodies' shape data (*16*). To plot and compare T_p on the same horizontal scale, a half-wavelength scale for the N-degree spherical harmonic function is introduced as $\lambda/2 = (2\pi R_p/2N)$ in place of N, where R_p is the body's radius. The relationship $T_p \propto (\lambda/2)$ for $\lambda/2 \geq 600$ km is generally confirmed for each body.

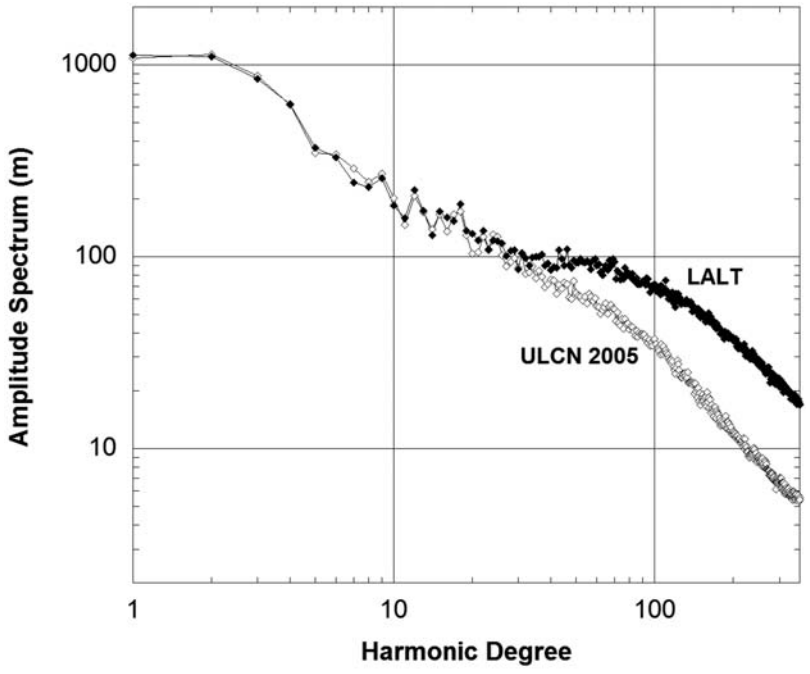

Fig. 3. Lunar topographic amplitude spectra from STM359_grid-02 (filled diamonds) and the spherical harmonic model from ULCN 2005 (open diamonds) (*4*). The two plots have similar characteristics for low-order coefficients. However, for scales smaller than 180 km, the Moon is clearly rougher than was previously known.

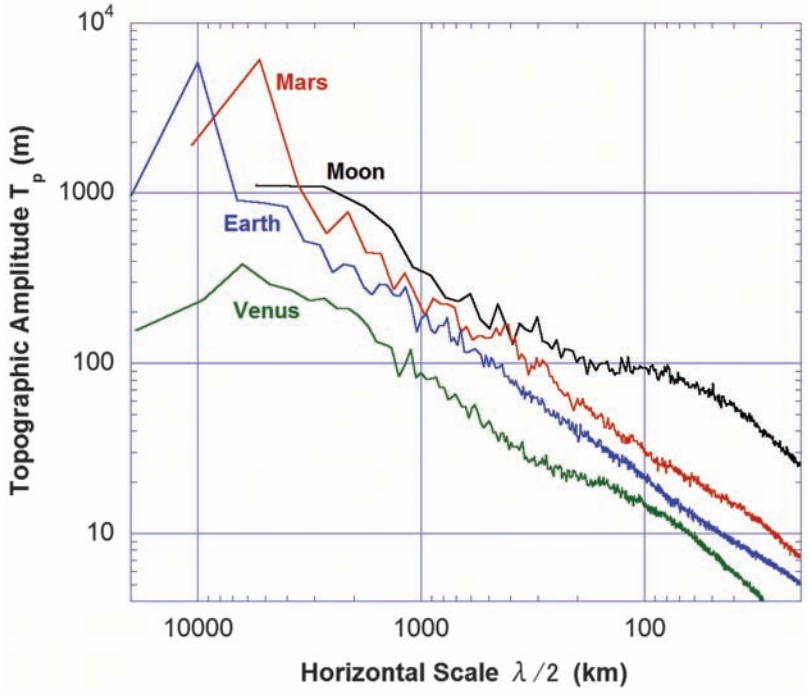

Fig. 4. Topographic amplitude spectra T_p for the Moon and three terrestrial planets. T_p is compared on the same horizontal scale $\lambda/2 = (2\pi R_p/2N)$, where R_p is the radius of each body.

The compensation state of Earth's interior is well explained by an Airy isostatic model. For the other three bodies, some degree of isostatic compensation is known to be achieved for the long-wavelength topography by comparing spectra of the observed and calculated gravity field, assuming that their short-wavelength topography is not compensated (*20*). Lunar free-air anomaly is moderate on the FHT or SPAT, where $\lambda/2$ is from 2000 to 4000 km, which indicates the isostatic equilibrium by the upwelling of the lower crust and/or upper mantle (*2*). However, T_M for $\lambda/2 \leq 400$ km exhibits a somewhat larger value than the prediction from the simple linear relationship [$T_M \propto (\lambda/2)$] and shows its virtually flat spectrum for 90 km $\leq \lambda/2 \leq 180$ km. These two characteristics contribute the excess of topographic spectrum for $\lambda/2 \leq 400$ km. A similar profile is observed for Venus (T_V), where the excess and flat spectrum is found for $\lambda/2 \leq 300$ km and 150 km $\leq \lambda/2 \leq 180$ km, respectively. For Mars (T_{Ma}), the excess spectrum is observed clearly for 400 km $\leq \lambda/2 \leq 600$ km and $\lambda/2 \cong 300$ km. The excess and/or flat spectrum common to the Moon, Venus, and Mars may indicate that the compensation mechanism by the buoyancy and elasticity of their lithosphere is changed to the simple rigid support. In the same way, the lack of such characteristics for the topographic spectra of Earth may suggest that the compensation mechanism is valid for Earth at least down to the topography whose horizontal scale is several tens of kilometers.

Why do the lithospheres of the Moon, Venus, and Mars seem to be more rigid for small-scale topography than Earth? The reason may be that volatile materials such as water, which weaken the mechanical property of the lithosphere, are relatively poor in the crust and/or upper mantle of these three bodies compared with Earth. It is confirmed that lunar surface rock does not have any signs of water or other volatile alteration, and the lunar lithosphere is considered to be extremely dry, which is probably the case for Venus, too, owing to its high-temperature surface environment (*21*). The interior of Mars may contain more water and other volatile materials than the Moon and Venus if we consider the hypothesis that a vast amount of liquid water had existed on its surface. However, based on the fact that no plate tectonics is observed on Mars, the water inside Mars would have very limited effects to weaken the rigidity of the lithosphere. In contrast, the water inside Earth plays an important role in the formation of the continents and in plate tectonics. Thus, the amount and activity of volatile materials within the terrestrial planets is considered to be a key parameter for understanding their global isostatic state as well as the mechanical properties of the lithosphere itself.

References and Notes

1. G. A. Neumann, *Int. Arch. Photogramm. Remote Sens.* **XXXIV-3** (W4), 73 (2001).
2. M. T. Zuber *et al.*, *Science* **266**, 1839 (1994).
3. D. E. Smith *et al.*, *J. Geophys. Res.* **102**, 1591 (1997).
4. B. A. Archinal *et al.*, "The Unified Lunar Control Network 2005" (Open-File Report 2006-1367 ver. 1.0, U.S. Geological Survey, 2006).
5. B. A. Campbell, D. B. Campbell, *Icarus* **180**, 1 (2006).
6. B. Bussey, P. Spudis, *The Clementine Atlas of the Moon* (Cambridge Univ. Press, Cambridge, 2004).
7. T. Tsubokawa *et al.*, *Proc. of the 23rd International Symposium on Space Technology and Science* (*ISTS*), Matsue Shimane, Japan, 26 May to 2 June 2002 (2002), pp. 1986–1991.
8. H. Araki *et al.*, *Adv. Space Res.* **42**, 317 (2008).
9. One remaining concern is about systematic errors in measurements of pulse arrivals due to distortion of the return pulse caused by the sloped and/or rough target terrain in combination with unknown albedo effects. This error (range shift) may result in underestimates of ranges by 12 m in the very worst case of 30° slope and 30% surface reflectance before the pulse spreading correction. For moderately flat surfaces, systematic range errors are expected to be 2.5 m (*8*).
10. D. E. Pavlis *et al.*, "GEODYN II system description, vols. 1-5," Contractor Report, SGT Inc. (2006).
11. J. J. McCarthy, "SOLVE program user's guide," Contractor Report between NASA/GSFC and Hughes/STX (2007).
12. N. Namiki *et al.*, *Science* **323**, 900 (2009).
13. Orbits are determined by full-scale precision force and measurement modeling. For each data arc, estimated parameters include the state vector at epoch, a solar radiation pressure coefficient, empirical accelerations with a once per orbital revolution signature in the along-track and cross-track direction, and measurement biases to absorb systematic effects and mismodeling. Orbit precision has been evaluated by computing orbit overlap differences. Overlap analysis showed a radial consistency of 1 m in general, with outliers (that were excluded from topography data processing) up to 4 m.
14. The pointing error is considered to be <0.1° (175 m for 100-km altitude), based on the thermal and other deformation analysis of the main orbiter. Time-tag error is <1 msec (1.5 m along-track for 100-km altitude) through the correction that takes into account the propagation time from the main orbiter to each station and the processing delay on each tracking station. These values (175 m and 1.5 m) are incorporated into the final budget as 3 SD errors.
15. The laser power has decreased since the middle of April 2008 for yet unexplained reasons, disrupting our data analysis schedule.
16. B. A. Archinal *et al.*, *Lunar Planet. Sci.* **XXXVIII**, 1904 (2007).
17. P. Wessel, W. H. F. Smith, *EOS* **72**, 441 (1991).
18. M. A. Wieczorek, in *Treatise on Geophysics*, G. Schubert, Ed. in Chief (Elsevier, Amsterdam, 2007), vol. 10, pp. 165–206.
19. P. K. Seidelmann *et al.*, *Celestial Mech. Dyn. Astron.* **98**, 155 (2007).
20. A. B. Watts, *Isostacy and Flexure of the Lithosphere* (Cambridge Univ. Press, Cambridge, 2001).
21. S. J. Mackwell *et al.*, *J. Geophys. Res.* **103**, 975 (1998).

22. We would like to express our great appreciation for the contributions of all staff engineers of NEC Co. Ltd. and the entire staff of the Kaguya (SELENE) project at JAXA in their development and operational support of LALT. We would also express our special thanks to M. Wieczorek for SHTOOLS on his Web site (www.ipgp.jussieu.fr/~wieczor) used for the spherical harmonic analysis and F. Lemoine and his colleagues at NASA Goddard Space Flight Center for invaluable discussions on the orbit accuracy of the Kaguya main orbiter. Finally, we are grateful to the reviewers for their helpful review and comments and to editors for their careful checking of our manuscript. All of the science data obtained by the Kaguya mission will be made available to the public in a PDS-like format (not PDS itself) via the Internet and/or some other method on 1 November 2009. LALT data sets are summarized in table S1.

Supporting Online Material

www.sciencemag.org/cgi/content/full/323/5916/897/DC1
Figs. S1 to S4
Table S1

4 August 2008; accepted 23 December 2008
10.1126/science.1164146

Farside Gravity Field of the Moon from Four-Way Doppler Measurements of SELENE (Kaguya)

Noriyuki Namiki,[1]* Takahiro Iwata,[2] Koji Matsumoto,[3] Hideo Hanada,[3] Hirotomo Noda,[3] Sander Goossens,[3] Mina Ogawa,[4] Nobuyuki Kawano,[3] Kazuyoshi Asari,[3] Sei-itsu Tsuruta,[3] Yoshiaki Ishihara,[3] Qinghui Liu,[3] Fuyuhiko Kikuchi,[3] Toshiaki Ishikawa,[3] Sho Sasaki,[3] Chiaki Aoshima,[5] Kosuke Kurosawa,[6] Seiji Sugita,[6] Tadashi Takano[7]

The farside gravity field of the Moon is improved from the tracking data of the Selenological and Engineering Explorer (SELENE) via a relay subsatellite. The new gravity field model reveals that the farside has negative anomaly rings unlike positive anomalies on the nearside. Several basins have large central gravity highs, likely due to super-isostatic, dynamic uplift of the mantle. Other basins with highs are associated with mare fill, implying basalt eruption facilitated by developed faults. Basin topography and mantle uplift on the farside are supported by a rigid lithosphere, whereas basins on the nearside deformed substantially with eruption. Variable styles of compensation on the near- and farsides suggest that reheating and weakening of the lithosphere on the nearside was more extensive than previously considered.

In the beginning of the space age, Apollo missions and their precursors discovered that the topography and crustal thickness of the Moon differed on the near and farsides (*1*). Post-Apollo global mapping missions such as Clementine, Lunar Prospector (LP) and Small Missions for Advanced Research in Technology–1 (SMART-1) further revealed that the near and farsides also differ in their chemical composition (*2*–*4*), which might be a consequence of asymmetric crystallization of a primordial magma ocean (*5*). Here, we present gravity data of the farside from SELENE (Kaguya) (*6*), which helps resolve the origin of this dichotomy.

The gravity field is a fundamental physical quantity for the study of the internal structure and the evolution of planetary bodies. The Moon was the first target of planetary gravimetry. In 1966, the Luna 10 mission began the study of the gravity field from observed orbital motion of the spacecraft. It was followed by Lunar Orbiter missions (LO) from I to V and Apollo 15 and 16 subsatellites (A15/16ss), and more recently Clementine and LP. Muller and Sjogren (*7*) discovered large positive gravity anomalies called "mascons" within maria basins on the nearside. The elliptic orbit of the Clementine spacecraft improved the lower degrees and sectorial terms of the gravity field (*8*). The low circular, polar orbit of LP increased the spatial resolution of the nearside gravity field (*9*), and we will use the degree and order 100 model (LP100K) (*9*) for comparisons with our model.

The most important problem of the previous lunar gravity models is the lack of direct observa-

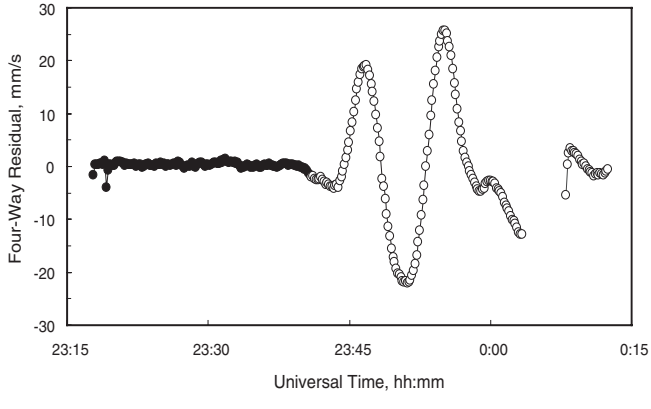

Fig. 1. Four-way Doppler residuals in pass from 23:17 UT on 5 November to 0:12 UT on 6 November 2007. Solid and open symbols indicate the visibility and invisibility of Main from UDSC, respectively. Four-way data are separated into two arcs by unloading of momentum wheels between 00:03 and 00:08.

[1]Kyushu University, 6-10-1 Hakozaki, Higashi-ku, Fukuoka 812-8581, Japan. [2]Institute of Space and Astronautical Science, Japan Aerospace Exploration Agency, 3-1-1 Yoshinodai, Sagamihara, Kanagawa 229-8510, Japan. [3]National Astronomical Observatory of Japan, 2-12 Hoshigaoka, Mizusawa, Oshu, Iwate 023-0861, Japan. [4]Japan Aerospace Exploration Agency, Tsukuba Space Center, 2-1-1 Sengen, Tsukuba, Ibaraki 305-8505, Japan. [5]Fujitsu Ltd., 1-9-3 Nakase, Mihama-ku, Chiba 261-8588, Japan. [6]University of Tokyo, 5-1-5 Kashiwanoha, Kasiwa, Chiba 277-8561, Japan. [7]Nihon University, 7-24-1 Narashinodai, Funabashi, Chiba 274-8501, Japan.

*To whom correspondence should be addressed. E-mail: nori@geo.kyushu-u.ac.jp

Lunar Global Shape and Polar Topography Derived from Kaguya-LALT Laser Altimetry

H. Araki, S. Tazawa, H. Noda, Y. Ishihara, S. Goossens, S. Sasaki, N. Kawano, I. Kamiya, H. Otake, J. Oberst and C. Shum

Science **323** (5916), 897-900.
DOI: 10.1126/science.1164146